Weak-Field Hall Resistivity and Spin-Valley Flavor Symmetry Breaking in Magic-Angle Twisted Bilayer Graphene

Ming Xie and A. H. MacDonald
Physics Department, University of Texas at Austin, Austin, Texas 78712, USA

(Received 16 October 2020; revised 27 July 2021; accepted 7 October 2021; published 2 November 2021)

Near a magic twist angle, the lowest energy conduction and valence bands of bilayer graphene moiré superlattices become extremely narrow. The band dispersion that remains is sensitive to the moiré's strain pattern, nonlocal tunneling between layers, and filling-factor-dependent Hartree and exchange band renormalizations. In this Letter, we analyze the influence of these band-structure details on the pattern of flavor symmetry breaking observed in this narrow band system and on the associated pattern of Fermi surface reconstructions revealed by weak-field Hall and Shubnikov–de Haas magnetotransport measurements.

DOI: 10.1103/PhysRevLett.127.196401

Introduction.—When twisted close to a magic [1] orientation angle, the ground state of bilayer graphene exhibits [2–5] a rich series of strongly correlated electronic ground states. The magic-angle twisted bilayer graphene (MATBG) phase diagram is most strongly dependent on twist angle θ and on moiré band filling factor $\nu = nA_M$, where n is the carrier density and A_M is the area of the moiré pattern unit cell, but is also responsive to other external parameters, including the orientation angles of the encapsulating hexagonal boron nitride layers and the vertical separation between the bilayer and the electrical gate or gates used to manipulate the carrier density.

Experimental work over the past couple of years [5–15] has established that the spin-valley flavor symmetries responsible for the fourfold degeneracy of the moiré bands are often broken when the flat conduction band is partially occupied or the flat valence band is partially emptied. The flavor symmetry breaking is reminiscent of the behavior of Bernal-stacked bilayer graphene in a strong magnetic field when its flat $N = 0$ Landau levels are partially filled [16–23]. The pattern of symmetry breaking is, however, quite distinct in the two cases. Instead of filling up the eight bands one at a time to minimize the exchange energy, as observed in the quantum Hall case, the flavor symmetry breaking in MATBG has a different guiding principle, which is illustrated schematically in Fig. 1. The broken symmetry states in MATBG almost always conspire to keep the partial filling factors $\nu_{\rm FS}$ of all flavors with a valence band Fermi surface above a critical value $\nu_v^{\rm cr}$, typically ∼0.55, and those of all flavors with a conduction band Fermi surface below $\nu_c^{\rm cr} \sim 0.2$. The observations from which this general rule is abstracted are briefly surveyed in the Supplemental Material [24]. Because the maximum conduction band electron Fermi surface areas are smaller than the maximum valence band hole Fermi surface areas, flavor symmetry breakings are more abundant on the conduction band side than on the valence band side. In this Letter, we provide an explanation for this behavior that is based on the influence of strain, nonlocal tunneling between layers, and filling-factor-dependent Hartree and exchange interactions on the band structure. Our analysis is

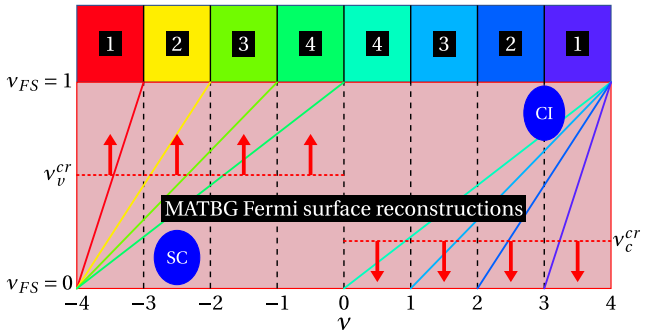

FIG. 1. The flat bands of MATBG are partially occupied for filling factor $\nu \in (-4, 4)$ and exhibit flavor symmetry breaking over much of this range. While not entirely universal, flavor symmetry breaking tends to follow the following rules. For negative carrier density, flavor symmetry breaking depopulates flat valence bands so as to keep the partial filling factors $\nu_{\rm FS}$ of the remaining partially occupied flavors, which have a Fermi surface, above $\nu_v^{\rm cr} \sim 0.55$, as indicated by the red arrows. For positive carrier densities, flavor symmetry breaking favors complete occupation of one, two, or three conduction bands so as to keep $\nu_{\rm FS}$ of the remaining partially occupied flavors below $\nu_c^{\rm cr} \sim 0.2$. The solid lines plot the band filling factor per partially occupied flavor in 1, 2, 3, and 4 Fermi surface states. This pattern of flavor symmetry breaking allows for insulating states at all nonzero ν between −4 and 4, and for Chen insulators (CIs) at odd integer ν. The strongest superconductivity (SC) seems to emerge from states with two valence band Fermi surfaces, and the strongest anomalous Hall effects seem to occur in states with one conduction band Fermi surface.

informed by Shubnikov–de Haas and weak-field Hall magnetotransport data [2,4–7,14,25–32].

MATBG band structure.—Magic-angle strong correlation physics persists over a small range of twist angles, covering perhaps ∼0.2°, within which the typical velocity within the flat bands is reduced by an order of magnitude or more relative to the band velocity in an isolated graphene layer. We argue here, however, that the band dispersion that survives near the magic twist angle plays a crucial role in establishing the ground state phase diagram.

We specify the single-particle MATBG flat bands using four phenomenological parameters: w_{AB}, the interlayer intersublattice tunneling strength; w_{AA}, the interlayer intrasublattice tunneling strength; a tunneling nonlocality parameter $w_{\rm NL}$; and ϵ^{-1}, a parameter that characterizes how strongly the moiré band Hamiltonian is modified by interactions. The spinless single-particle Hamiltonian projected onto valley K takes the form

$$\hat{\mathcal{H}}^{K}_{\rm sp} = \begin{pmatrix} h_{\theta/2}(\boldsymbol{k}) & T(\boldsymbol{r},\boldsymbol{r}') \\ T^{\dagger}(\boldsymbol{r},\boldsymbol{r}') & h_{-\theta/2}(\boldsymbol{k}') \end{pmatrix}, \tag{1}$$

where $\hat{h}_{\pm\theta/2}$ are the Dirac Hamiltonians for isolated rotated graphene top (+) and bottom (−) layers and $T(\boldsymbol{r},\boldsymbol{r}')$ is the interlayer tunneling term. The ratio w_{AA}/w_{AB} has the value 1 for simplified models [1] in which the graphene layers are rotated rigidly, but is known [33–35] to be reduced relative to 1 when strain and corrugation are taken into account. The nonlocality of the interlayer tunneling is known [34,36,37] to be principally responsible for particle-hole asymmetry in MATBG, which we model by setting

$$T(\boldsymbol{r},\boldsymbol{r}') = \sum_{j=0}^{2}\sum_{\boldsymbol{p}} T_j(\boldsymbol{p}) e^{-i\boldsymbol{q}_j\cdot(\boldsymbol{r}+\boldsymbol{r}')/2} e^{i\boldsymbol{p}\cdot(\boldsymbol{r}-\boldsymbol{r}')}, \tag{2}$$

where $T_j(\boldsymbol{p}) = t(\boldsymbol{p})T_j^{\rm BM}$ and the momentum-dependent tunneling amplitude $t(\boldsymbol{p}) = t_{k_D} + (dt/dp)_{p=k_D}(k_D - p)$. We parametrize the slope of the momentum dependence in $t(\boldsymbol{p})$ by $w_{\rm NL} \equiv (dt/dp)_{p=k_D}|\boldsymbol{b}|$. We note that $T(\boldsymbol{r},\boldsymbol{r}') = T(\boldsymbol{r})\delta(\boldsymbol{r},\boldsymbol{r}')$ is local in the Bistritzer-MacDonald (BM) model, where the tunneling matrix $T_j^{\rm BM} = \omega_{AA}/\omega_{AB} + \cos(j\phi)\sigma_x + \sin(j\phi)\sigma_y$ is independent of momentum (see Supplemental Material [24]). Below we explain what magnetotransport measurements tell us about the typical values of these band parameters.

The flat bands of MATBG have a simple and systematic dependence on band filling, one that we argue plays an important role in the flat band phase diagram. In Fig. 2, we plot the flat bands when they are completely full and when they are empty. These calculations neglect mixing between flat and remote bands, an approximation that is justified by flat band spectral isolation. In this approximation, the many-electron ground state is fully determined by the Pauli exclusion principle in both limits and is a single Slater determinant in which single-particle-state occupation numbers are either 0 or 1. It follows that the electron self-energy is given exactly by the Hartree-Fock operator

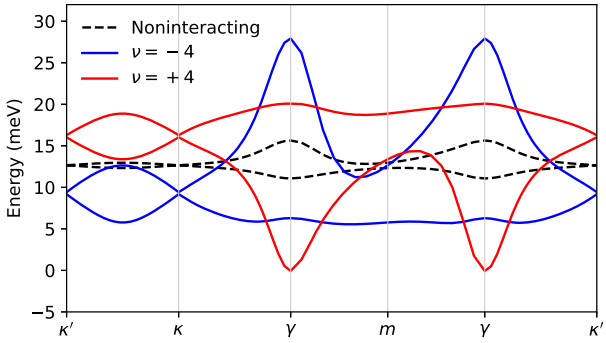

FIG. 2. Band structures in the full and empty moiré band limits for band parameters $\hbar v k_\theta = 1.69 w_{AB}$, corresponding to a twist angle of about $\theta \sim 1.1°$. $w_{AA}/w_{AB} = 0.6$, $w_{\rm NL} = 20$ meV, and $\epsilon^{-1} = 0.03$. Interaction effects strongly weaken dispersion when the Fermi level moves toward γ on either electron or hole sides.

$$\hat{\Sigma}^{\rm HF} = \hat{\Sigma}^{\rm H}(\delta\rho) + \hat{\Sigma}^{\rm F}(\delta\rho), \tag{3}$$

where $\delta\rho = \sum'_{\alpha,n,\boldsymbol{k}} |\alpha,n,\boldsymbol{k}\rangle\langle\alpha,n,\boldsymbol{k}| - \rho_{\rm iso}$ is the ground state density matrix defined relative to neutral isolated graphene states, α is a composite label for valley and spin, n is a single-particle band label, the prime restricts the summation to filled bands, and $\hat{\Sigma}^{\rm H}$ and $\hat{\Sigma}^{\rm F}$ are the usual Hartree and Fock self-energies (see Supplemental Material [24] for further details.) In Fig. 2 we have used $\epsilon^{-1} = 0.03$ to account [38] for screening by the surrounding dielectric, by the two-dimensional material itself, and by the gates.

The bands plotted in Fig. 2 are eigenvalues of the band Hamiltonian $\hat{\mathcal{H}}_{\mathcal{B}} = \hat{\mathcal{H}}_{\rm sp} + \hat{\Sigma}^{\rm HF}$, where $\hat{\mathcal{H}}_{\rm sp}$ is the single-particle moiré band Hamiltonian. The difference between the quasiparticle dispersions in the empty and full band limits is due to the differences between the self-energy operator when the flat bands are full $\hat{\Sigma}^{\rm HF}_f$ and when the flat bands are empty $\hat{\Sigma}^{\rm HF}_e$. We see in Fig. 2 that the effect of the self-energy is to lower (raise) the energy near the center of the moiré Brillouin zone ($\boldsymbol{k} = \boldsymbol{\gamma}$), relative to those near the corners of the Brillouin zone ($\boldsymbol{k} = \boldsymbol{\kappa}, \boldsymbol{\kappa}'$) as the flat conduction (valence) bands are filled (emptied). This behavior has been explained [39,40] in terms of Hartree interactions and the concentration of flat band states at AA positions in the bilayer moiré pattern, where the wave functions of flat band states near $\boldsymbol{\gamma}$ have lower weight [41,42]. Exchange interactions also play a role in reshaping the bands and a more critical role in breaking flavor symmetries (see [39] and Supplemental Material [24]). These interaction effects have a smooth dependence on filling factor, which justifies the approximation

$$\hat{\mathcal{H}}_{\mathcal{B}} = \hat{\mathcal{H}}_{\rm sp} + \frac{1}{2}[\hat{\Sigma}_f^{\rm HF} + \hat{\Sigma}_e^{\rm HF} + \frac{\nu}{4}(\hat{\Sigma}_f^{\rm HF} - \hat{\Sigma}_e^{\rm HF})]. \quad (4)$$

The end result is that Fermi velocities are extremely small when the bands are nearly empty and nearly full, in contrast to the case of single-particle band models for which Fermi velocities are maximized for nearly full and nearly empty bands. This property is captured only when self-energies from frozen remote bands are included in the theory. We argue below that it also plays a crucial role in determining the pattern of flavor symmetry breaking.

Shubnikov–de Haas oscillations.—Oscillations in physical properties associated with periodic filling and emptying of nascent Landau levels in weak magnetic fields have long [43] been used to measure the Fermi surfaces of metals. In two-dimensional materials, the most accessible oscillations are normally those of longitudinal resistance referred to as Shubnikov–de Haas (SdH) oscillations. SdH oscillations in MATBG [2,4–7,14,25–32] are, generally speaking, observable only near neutrality for $\nu \in (-1.6, 0.8)$ and for $|\nu| \in (2, 3)$. We attribute this property to the interaction-induced reductions in Fermi velocity when the bands are nearly empty or nearly full as explained above. Comparison of Fermi surface area to carrier density suggests that all four flavors have equivalent Fermi surfaces near neutrality. For $|\nu| \in (2, 3)$, the same comparison suggests that only two of the four flavors have Fermi surfaces, the other two flat bands having apparently been depopulated on the valence band side and completely filled on the conduction band side. These observations are consistent with the interpretation of weak-field Hall observations discussed below, which are able to provide valuable information over the full range of flat band filling factors because they do not rely on an adequate Landau level spacing.

Weak-field Hall resistivity.—When mean free paths exceed Fermi wavelengths, the transport properties of two-dimensional Fermi liquids can be described using Boltzmann transport theory. Employing a relaxation time approximation, a practical necessity when the source of scattering is unknown, the conductivity tensor of a system with C_6 symmetry is given [44] to leading order in magnetic field B by

$$\sigma_{xx} = e^2\tau \sum_{\boldsymbol{k}} \left(-\frac{\partial f_{\boldsymbol{k}}}{\partial E}\right) v_x^2,$$
$$\sigma_{yx} = \frac{2e^3\tau^2 B}{\hbar} \sum_{\boldsymbol{k}} \left(-\frac{\partial f_{\boldsymbol{k}}}{\partial E}\right) v_x(\boldsymbol{v}\times\boldsymbol{z})\cdot\boldsymbol{\nabla} v_y,$$
$$\sigma_{xx} = \sigma_{yy}, \sigma_{yx} = -\sigma_{xy}. \quad (5)$$

It follows that, to first order in B, the Hall resistivity

$$\rho_{xy} = \frac{\sigma_{yx}}{\sigma_{xx}^2} \equiv \frac{B}{n_H e c}. \quad (6)$$

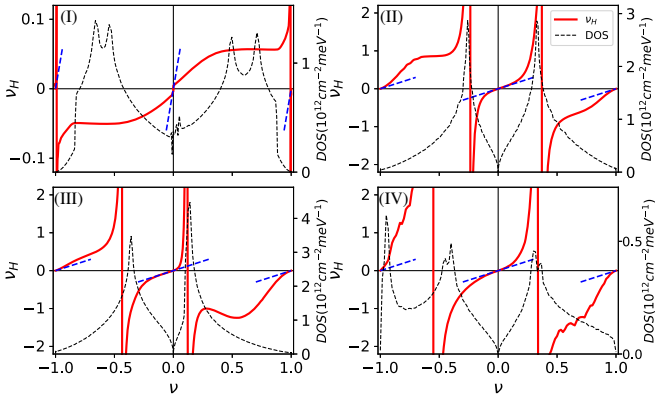

FIG. 3. Hall filling factor $\nu_H = n_H A_M$ vs band filling factor ν of a single flavor for the band models (I–IV) defined in the main text. In numerical order, the four models improve the BM model (I) by sequentially adding corrections for strain (II), nonlocal tunneling (III), and interactions (IV). The black dashed curves plot the band DOS, whose peaks are located at the vHS energies. The blue dashed lines are the Hall densities $\nu_H = \nu + 1, \nu, \nu - 1$ for isotropic Fermi surfaces near $\nu = -1$, 0, 1, respectively.

In Eq. (6), the coefficient of the B-linear term in ρ_{xy} is a pure band-structure property because the scattering time τ cancels between numerator and denominator. As suggested by the final form on the right-hand side, it is convenient to characterize this quantity by the Hall density n_H, which is defined by this equation. $|n_H|$ equals the carrier density for isotropic Fermi surfaces [44].

In Fig. 3, we plot Hall filling factor $\nu_H = n_H A_M$ vs filling factor ν for partially occupied MATBG bands at $w_{AB}/\hbar v K = 1.69$ for four different band-structure models: (I) $w_{AA} = w_{AB}$, $w_{\rm NL} = 0$, (II) $w_{AA}/w_{AB} = 0.6$, $w_{\rm NL} = 0$, (III) $w_{AA}/w_{AB} = 0.6$, $w_{\rm NL} = 20$ meV, and (IV) $w_{AA}/w_{AB} = 0.6$, $w_{\rm NL} = 20$ meV with $\epsilon^{-1} = 0.03$. The first model is the BM model specified in [1], which is improved in models II–IV by sequentially adding corrections for strain and corrugation, nonlocal tunneling, and interactions. In all cases, $\nu_H \sim \nu$ close to neutrality, expected for isotropic Fermi surfaces. Away from neutrality, Fermi surfaces are more anisotropic for larger ω_{AA}/ω_{AB} and this leads to larger deviations [44] of the Hall density from the corresponding Fermi surface area curves marked in blue. (The sensitivity of the Hall density to band parameters is discussed in detail in the Supplemental Material [24].)

The most prominent features in Fig. 3 are the switches between large ν_H's of opposite signs that occur once for positive and once for negative filling factors. The filling factors at which these sign changes occur are close to the filling factors at which the topology of the Fermi surfaces changes from electron- to holelike. As explained in the Supplemental Material [24], the sign changes do not precisely match the van Hove singularities (vHSs) at which the flat band density of states (DOS) diverges logarithmically yielding a feature that is prominent in tunneling

spectroscopy measurements [8–12]. We see in Fig. 3 that the positions of these sign changes are sensitive to the band-structure model details. They move very close to neutrality when the strain and corrugation corrections are added. Including nonlocal tunneling shifts the position closer to (further from) neutrality on the conduction (valence) band side, strongly violating particle-hole symmetry. Interaction renormalizations move the sign change positions on both sides away from neutrality by an amount determined by the strength of interaction.

Hall density, Fermi surface reconstruction, and Lifshitz transitions.—The Hall densities in Fig. 3 differ qualitatively from experimental data, which typically exhibit five or more jumps in value for $\nu \in (-4, 4)$ compared to the two jumps present in Fig. 3 assuming no flavor symmetry breaking. Some of these jumps are evidently due to spin-valley flavor symmetry breaking phase transitions, which reconstruct the Fermi surfaces. These transitions sequentially maximize hole densities for one, two, or three flavors on the hole side and electron densities of one, two, or three flavors on the conduction band side. The guiding principle for these phase transitions seems to be to place the Fermi levels of the partially occupied bands, whenever possible, on the side of the van Hove singularity closer to the Dirac point of that flavor. We can understand this behavior [45] qualitatively as a combined consequence of the exchange energy gained by flavor polarization and the favorable band energy per particle when the Fermi level is placed in the low-DOS region near the Dirac point.

The number of additional Hall density jumps and their precise filling-factor positions are somewhat sample dependent. Figure 4 shows calculated Hall density that accounts for flavor symmetry breaking transitions. The second Hall density jump on the valence band side is consistent with traversal of vHSs in doubly degenerate Fermi surfaces. On the conduction band side, the first Hall density jump occurs already near $\nu \approx 4\nu_c^{\mathrm{cr}}$. We attribute the difference between electrons and holes to the difference in the position at which the vHS occurs. Two additional jumps in Hall density typically occur on the conduction band side, and each seems to be associated with a flavor depopulation event. One important consequence is that states with an odd number of Fermi surfaces are more common on the conduction band side. We have constructed the theory curve in Fig. 4 from Fig. 3 by summing Hall conductivity contributions over flavors. As shown there, we are able to explain the experimental results by inferring that there is one flavor symmetry breaking transition on the hole side at $\nu_{\mathrm{FS}} \approx \nu_v^{\mathrm{cr}}$ [or, equivalently, $\nu \approx -4(1-\nu_v^{\mathrm{cr}})$] from a four-Fermi surface state to a two-Fermi surface state, and that there are three flavor symmetry breaking transitions on the electron side, at $\nu \approx 4\nu_c^{\mathrm{cr}}$, $1+3\nu_c^{\mathrm{cr}}$, and $2+2\nu_c^{\mathrm{cr}}$, to three, two, and one Fermi surface states. Because the Hall density curves are qualitatively dependent on the pattern of flavor symmetry breaking, as illustrated in the Supplemental Material [24], this interpretation can be made with considerable confidence.

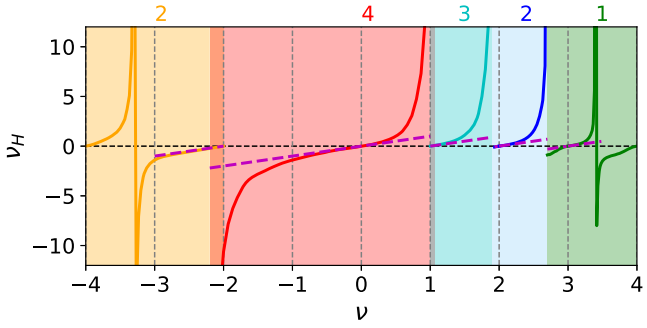

FIG. 4. Hall filling factor as a function of band filling factor allowing spin-valley flavor symmetry breaking, calculated using interaction renormalized bands and the pattern of flavor symmetry explained in the main text. The shading specifies the number of partially occupied bands, i.e., the number of Fermi surfaces in each region of filling factor. The solid lines mark the Hall density that would be calculated if the Fermi surfaces were approximated as isotropic.

The flavor symmetry breaking behavior evident in the weak-field Hall and SdH data is understandable in terms of mean-field considerations. States that have a Fermi level on the neutrality side of the vHS are favored by a low DOS close to the Fermi level [46]. Particle-hole asymmetry can be explained by the closer proximity of vHS to neutrality on the conduction band side, which forces flavor symmetry breaking earlier in the conduction band filling process than in the valence band emptying process, and therefore favors states with an odd number of Fermi surfaces that can host topologically nontrivial states [6,7,47].

Discussion.—This Letter addresses the implications of weak-field magnetotransport data for the correlation physics of MATBG. The moiré filling-factor ranges over which SdH oscillations are visible identify where Fermi level quasiparticles have the largest velocities. The fact that SdH oscillations are most visible near neutrality is at first sight surprising, since the independent electron flat bands are most dispersive in precisely the opposite limit, namely, for nearly full or nearly empty bands. We have interpreted this behavior as a consequence of interaction-induced band renormalizations that flatten the conduction band top and the valence band bottom when the Fermi level is near these band edges.

Weak-field Hall effect measurements provide additional information since this quantity is observable at larger quasiparticle masses and stronger disorder. We have concluded that the many jumps in Hall density that typically occur as a function of band filling cannot be explained on the basis of single-particle physics, since these allow for only one jump on each side of the neutrality point. We attribute the additional jumps to a series of flavor symmetry breaking phase transitions that reconstruct Fermi surfaces by redistributing the occupancy among flavors. These

reconstructions favor partially occupied bands whose Fermi surfaces are on the neutrality side of the vHS present in each band. A similar conclusion was reached on the basis of thermodynamic compressibility measurements in Ref. [13]. Our analysis argues that filling-factor-dependent band renormalizations play an essential role in the robustness of this effect and that nonlocal interlayer tunneling controls its particle-hole asymmetry, which is substantial in most cases.

Unlike a ferromagnetic metal, in which the spin dependence of electron-electron interactions is normally ignored, the valley and orbital dependence of interactions in MATBG could [48,49] play as important a role as the band Hamiltonian in the anisotropy energy scales and could play a role in the superconducting state that emerges at the lowest temperatures. Surveying the experimental literature and assigning Fermi surface degeneracies via considerations like those discussed in this Letter, it seems that superconductivity occurs with similar transition temperatures in states with two and four Fermi surfaces, but has much lower transition temperatures when seen in states with an odd number of Fermi surfaces.

The authors acknowledge helpful interactions with Eva Andrei, Dmitry Efetov, Wei Qin, Petr Stepanov, Shuang Wu, Andrea Young, and Zhenyuan Zhang. We thank Stephen Carr for a helpful conversation explaining the relationship between particle-hole asymmetry in the flat bands and tunneling nonlocality. This work was supported by the U.S. Department of Energy, Office of Science, Basic Energy Sciences, under Award No. DE-SC0022106.

[1] R. Bistritzer and A. H. MacDonald, Proc. Natl. Acad. Sci. U.S.A. **108**, 12233 (2011).
[2] Y. Cao, V. Fatemi, A. Demir, S. Fang, S. L. Tomarken, J. Y. Luo, J. D. Sanchez-Yamagishi, K. Watanabe, T. Taniguchi, E. Kaxiras, R. C. Ashoori, and P. Jarillo-Herrero, Nature (London) **556**, 80 (2018).
[3] Y. Cao, V. Fatemi, S. Fang, K. Watanabe, T. Taniguchi, E. Kaxiras, and P. Jarillo-Herrero, Nature (London) **556**, 43 (2018).
[4] M. Yankowitz, S. Chen, H. Polshyn, K. Watanabe, T. Taniguchi, D. Graf, A. F. Young, and C. R. Dean, Science **363**, 1059 (2019).
[5] X. Lu, P. Stepanov, W. Yang, M. Xie, M. A. Aamir, I. Das, C. Urgell, K. Watanabe, T. Taniguchi, G. Zhang, A. Bachtold, A. H. MacDonald, and D. K. Efetov, Nature (London) **574**, 653 (2019).
[6] A. L. Sharpe, E. J. Fox, A. W. Barnard, J. Finney, K. Watanabe, T. Taniguchi, M. A. Kastner, and D. Goldhaber-Gordon, Science **365**, 605 (2019).
[7] M. Serlin, C. L. Tschirhart, H. Polshyn, Y. Zhang, J. Zhu, K. Watanabe, T. Taniguchi, L. Balents, and A. F. Young, Science **367**, 900 (2020).
[8] Y. Jiang, X. Lai, K. Watanabe, T. Taniguchi, K. Haule, J. Mao, and Eva Y. Andrei, Nature (London) **573**, 91 (2019).
[9] A. Kerelsky, L. McGilly, D. M. Kennes, L. Xian, M. Yankowitz, S. Chen, K. Watanabe, T. Taniguchi, J. Hone, C. Dean, A. Rubio, and A. N. Pasupathy, Nature (London) **572**, 95 (2019).
[10] Y. Xie, B. Lian, B. Jäck, X. Liu, C.-L. Chiu, K. Watanabe, T. Taniguchi, B. A. Bernevig, and A. Yazdani, Nature (London) **572**, 101 (2019).
[11] Y. Choi, J. Kemmer, Y. Peng, A. Thomson, H. Arora, R. Polski1, Y. Zhang, H. Ren, J. Alicea, G. Refael, F. von Oppen, K. Watanabe, T. Taniguchi, and S. Nadj-Perge, Nat. Phys. **15**, 1174 (2019).
[12] D. Wong, K. P. Nuckolls, M. Oh, B. Lian, Y. Xie, S. Jeon, K. Watanabe, T. Taniguchi, B. Andrei Bernevig, and A. Yazdani, Nature (London) **582**, 198 (2020).
[13] U. Zondiner, A. Rozen, D. Rodan-Legrain, Y. Cao, R. Queiroz, T. Taniguchi, K. Watanabe, Y. Oreg1, F. von Oppen, Ady Stern, E. Berg, P. Jarillo-Herrero, and S. Ilani, Nature (London) **582**, 203 (2020).
[14] P. Stepanov, I. Das, X. Lu, A. Fahimniya, K. Watanabe, T. Taniguchi, F. H. L. Koppens, J. Lischner, L. Levitov, and D. K. Efetov, Nature (London) **583**, 375 (2020).
[15] C. L. Tschirhart, M. Serlin, H. Polshyn, A. Shragai, Z. Xia, J. Zhu, Y. Zhang, K. Watanabe, T. Taniguchi, M. E. Huber, and A. F. Young, Science **372**, 1323 (2021).
[16] E. McCann and V. I. Fal'ko, Phys. Rev. Lett. **96**, 086805 (2006).
[17] Y. Barlas, R. Côté, K. Nomura, and A. H. MacDonald, Phys. Rev. Lett. **101**, 097601 (2008).
[18] R. Côté, W. Luo, B. Petrov, Y. Barlas, and A. H. MacDonald, Phys. Rev. B **82**, 245307 (2010).
[19] J. Jung, F. Zhang, and A. H. MacDonald, Phys. Rev. B **83**, 115408 (2011).
[20] Y. Barlas, K. Yang, and A. H. MacDonald, Nanotechnology **23**, 052001 (2012).
[21] B. E. Feldman, J. Martin, and A. Yacoby, Nat. Phys. **5**, 889 (2009).
[22] J. Martin, B. E. Feldman, R. T. Weitz, M. T. Allen, and A. Yacoby, Phys. Rev. Lett. **105**, 256806 (2010).
[23] R. T. Weitz, M. T. Allen, B. E. Feldman, J. Martin, and A. Yacoby, Science **330**, 812 (2010).
[24] See Supplemental Material at http://link.aps.org/supplemental/10.1103/PhysRevLett.127.196401 for a survey of published experimental observations from weak-field Hall and SdH oscillation measurements, a detailed description of the effective nonlocal tunneling model, the relation between Fermi surface topology and weak-field Hall resistivity, and details of Hartree-Fock self-energies.
[25] S. Wu, Z. Zhang, K. Watanabe, T. Taniguchi, and E. Y. Andrei, Nat. Mater. **20**, 488 (2021).
[26] H. S. Arora, R. Polski, Y. Zhang, A. Thomson, Y. Choi, H. Kim, Z. Lin, I. Z. Wilson, X. Xu, J.-H. Chu, K. Watanabe, T. Taniguchi, J. Alicea, and S. Nadj-Perge, Nature (London) **583**, 379 (2020).
[27] A. Uri, S. Grover, Y. Cao, J. A. Crosse, K. Bagani, D. Rodan-Legrain, Y. Myasoedov, K. Watanabe, T. Taniguchi, P. Moon, M. Koshino, P. Jarillo-Herrero, and E. Zeldov, Nature (London) **581**, 47 (2020).
[28] I. Das, X. Lu, J. Herzog-Arbeitman, Z.-D. Song, K. Watanabe, T. Taniguchi, B. A. Bernevig, and D. K. Efetov, Nat. Phys. **17**, 710 (2021).

[29] Y. Saito, J. Ge, K. Watanabe, T. Taniguchi, and A. F. Young, Nat. Phys. **16**, 926 (2020).
[30] Y. Saito, J. Ge, L. Rademaker, K. Watanabe, T. Taniguchi, D. A. Abanin, and A. F. Young, Nat. Phys. **17**, 478 (2021).
[31] Y. Saito, F. Yang, J. Ge, K. Watanabe, X. Liu, T. Taniguchi, J. I. A. Li, E. Berg, and A. F. Young, Nature (London) **592**, 220 (2021).
[32] P. Stepanov, M. Xie, T. Taniguchi, K. Watanabe, X. Lu, A. H. MacDonald, B. A. Bernevig, and D. K. Efetov, arXiv:2012.15126.
[33] S. Carr, D. Massatt, S. B. Torrisi, P. Cazeaux, M. Luskin, and E. Kaxiras, Phys. Rev. B **98**, 224102 (2018).
[34] S. Carr, S. Fang, Z. Zhu, and E. Kaxiras, Phys. Rev. Research **1**, 013001 (2019).
[35] G. Tarnopolsky, A. J. Kruchkov, and A. Vishwanath, Phys. Rev. Lett. **122**, 106405 (2019).
[36] S. Fang, S. Carr, Z. Zhu, D. Massatt, and E. Kaxiras, arXiv:1908.00058.
[37] F. Guinea and N. R. Walet, Phys. Rev. B **99**, 205134 (2019).
[38] J. Zhu, M. Xie, and A. H. MacDonald (to be published).
[39] M. Xie and A. H. MacDonald, Phys. Rev. Lett. **124**, 097601 (2020).
[40] F. Guinea and N. R. Walet, Proc. Natl. Acad. Sci. U.S.A. **115**, 13174 (2018).
[41] H. C. Po, L. Zou, T. Senthil, and A. Vishwanath, Phys. Rev. B **99**, 195455 (2019).
[42] Z. Song, Z. Wang, W. Shi, G. Li, C. Fang, and B. A. Bernevig, Phys. Rev. Lett. **123**, 036401 (2019).
[43] David Schoenberg, *Magnetic Oscillations in Metals* (Cambridge University Press, Cambridge, England, 1984).
[44] N. P. Ong, Phys. Rev. B **43**, 193 (1991).
[45] M. Xie, W. Qin, and A. H. MacDonald (to be published).
[46] The even lower DOS interval that occurs for nearly full and nearly empty bands when interactions are neglected does not share the enhanced stability of its Dirac point cousin because of interaction renormalizations that reduce Fermi velocities when bands are nearly full or nearly empty.
[47] K. P. Nuckolls, M. Oh, D. Wong, B. Lian, K. Watanabe, T. Taniguchi, B. A. Bernevig, and A. Yazdani, Nature (London) **588**, 610 (2020).
[48] N. Bultinck, E. Khalaf, S. Liu, S. Chatterjee, A. Vishwanath, and M. P. Zaletel, Phys. Rev. X **10**, 031034 (2020).
[49] J. Liu and X. Dai, Phys. Rev. B **103**, 035427 (2021).